J Electroceram (2012) 28:109–117
DOI 10.1007/s10832-012-9690-y

Electrical and structural characterization of PTCR pure $BaTiO_3$ nanopowders synthesized by sol–gel emulsion technique

Zubeda Bi H. Aga · Sutapa Roy Ramanan

Received: 25 August 2011 / Accepted: 1 February 2012 / Published online: 12 February 2012

Abstract $BaTiO_3$ ceramics have been widely studied for its application as multilayer ceramic capacitors. However, they have been reported to deviate from their insulating to semiconducting behavior upon doping, and are used as positive temperature coefficient (PTC) thermistors and transducers. In this work, sol–gel emulsion technique was used for synthesis of $BaTiO_3$ powders of various shapes and sizes. The synthesized powders were calcined at two different temperatures i.e. 750°C, and 1000°C. XRD revealed the powders to be primarily cubic in structure. Presence of tetragonality was noted in the powders calcined at 1000°C. Crystallite size was calculated for the powders calcined at 750°C and 1000°C. Average particle size of the prepared powders varied from 42 to 94 nm. The shape and size of the particles were dependent on the type and concentration of the surfactant used. The synthesized material showed positive temperature coefficient of resistivity (PTCR) behavior. From the recorded resistivity values a maximum of 10^{10} Ωcm was achieved. The ferroelectric to paraelectric transition temperature, Curie point, (T_c) was found to be at 75°C from the impedance spectroscopy analysis for the prepared material.

Keywords $BaTiO_3$ · Sol–gel emulsion · Surfactant · Tetragonality · PTCR

1 Introduction

Barium titanate based ceramics exhibit a wide variety of electrical phenomena which are used in applications such as sensors and actuators [1]. There are five polymorphs attributed to barium titanate ($BaTiO_3$) namely; hexagonal, cubic, tetragonal, orthorhombic and rhombohedral with the transition temperature at 1460°C, 120°C, 0°C and −90°C. Among which the most widely studied is the tetragonal (ferroelectric) structure that is stable from 0°C to 120°C [2–7]. From a transducer, its major application in the field of electronic industry today is in the form of a capacitor due to its high permittivity and easy modification of electronic properties. Other applications include resonators, filter-duplexers, voltage-controlled oscillators, antennas etc. [8, 9]. Pure $BaTiO_3$ has resistivity values greater than 10^{12} Ωcm, characteristic of an insulator [10, 11]. On being doped with donors, this insulating material becomes semiconducting (resistivity range of 10^{-4} to 10^{10} Ωcm) and shows a PTCR (Positive temperature coefficient of resistivity) behavior. Resistivity value as low as 10 Ωcm at ambient has been achieved for semiconducting $BaTiO_3$ [9, 10, 12]. PTCR is the electrical response of materials such as $BaTiO_3$, wherein, its resistivity increases abruptly at the transition temperature (T_c) and is much greater than its room temperature value. This increase in resistivity is ascribed to an increase in the potential barrier at the grain boundaries which is inversely related to the dielectric constant of the material by the Curie –Weiss law above T_c. Above T_c, this increase in resistivity is noted up to a temperature where the potential barriers saturate followed by a decrease due to which the resistivity of the material starts decreasing lending it a negative temperature coefficient of resistivity (NTCR) behavior [13]. Therefore a PTCR $BaTiO_3$ has an initial NTCR behavior up to T_c above which it shows a PTCR and then again an NTCR behavior [14–16]. These $BaTiO_3$ ceramics exhibiting PTCR behavior are used as PTC thermistors for current overload protection devices, thermal fuses and temperature sensors [9].

Z. B. H. Aga · S. R. Ramanan (✉)
Department of Chemical Engineering, BITS, Pilani,
K. K. Birla Goa Campus,
Zuarinagar, Goa, India
e-mail: sutapa@bits-goa.ac.in

Different synthesis techniques such as solid state method, hydrothermal method, co-precipitation method, sol–gel method, etc. have been employed in the synthesis of $BaTiO_3$ powders. An extensive study of synthesis technique and the starting materials has been carried out by various authors because of the influence it has on the quality of the synthesized powders. Of these, the commercially used solid state method produces particles in the micro-meter range with presence of $BaCO_3$ even after calcinations at temperatures as high as 1400°C for several hours. Ferroelectric properties are highly dependent on the grain size, domain structure, and composition due to which control of processing conditions including thermal treatment are required [14, 17, 18]. Hence, wet chemical methods like sol–gel have been studied to generate highly pure, homogeneous, reactive ultrafine barium titanate powders [15, 16, 19].

Sol-precipitation, sol-crystal, microemulsion, sol-emulsion-gel, gel-sol process are developed refined sol–gel processes [20, 21]. Emulsion is a thermodynamically stable dispersion of a polar (water or an aqueous solution) and a non-polar (oil) solvent. Surface active agents, when added, adsorb at the interface of the two immiscible liquids to form droplets called micelles. These agents referred as surfactants have amphiphilic character consisting of a hydrophilic head group and one or two lipophilic/hydrophorbic (C-H-chain) tail group. In the water in oil (*w/o*) type emulsions with spherical nano-sized aqueous micelles (reverse/inverse micelle) dispersed in an oil matrix, the aqueous droplet can be used as nano-reactors and templates for the preparation of solid nano-particles [21, 22].

In the current paper, we have reported the synthesis of $BaTiO_3$ nanopowders by sol–gel emulsion technique. The electrical and structural properties of the synthesized powders are studied as a function of different process parameters.

2 Experimental procedure

$Ba(CH_3COO)_2.H_2O$, (Sisco Research Laboratory Pvt. Ltd., India), and Ti-isopropoxide (Merck, Germany) were used as the source of Ba and Ti respectively. Acetic acid and acetylacetone were used as the chelating agents. The molar ratio of acetic acid and acetylacetone to that of titanium alkoxide was 2.4 and 0.3 respectively. To a Ti-isopropoxide solution with acetic acid and acetyl acetone, a 1.5 M $Ba(CH_3COO)_2.H_2O$ solution in distilled water, maintaining a Ba/Ti atomic ratio of 1:1 was added dropwise under continuous stirring at ambient conditions. A clear translucent sol was obtained with no traces of precipitate formation.

The prepared sol (water medium) was dispersed under continuous stirring in a mixture called support solvent (comprising of cyclohexane (oil medium) with the desired amount of surfactant) to form *w/o* type emulsion. Two different sol:support solvent ratio, namely, 1:2 and 1:3 was studied with two different types of surfactant (Span 80 and 20). The surfactant concentration was changed as 5%, 10%, 15%, and 20% of the cyclohexane volume. Triethylamine was added to the emulsion as a gelling agent to transform the sol droplets to gel droplets. The addition was continued until a pH value of 9.0 was reached. The prepared gel droplets were washed with methanol, filtered, then dried at 100°C, and then calcined at 750°C and 1000°C. The results obtained were almost same for the two ratios. Hence, further experiments were carried out with the 1:3 sol: support solvent ratio.

The calcined powders were analyzed using an X-ray diffractometer (Rigaku, Miniflex II), Thermogravimetric Analyser (DTG-60,Shimadzu), Differential Scanning Calorimetry (DSC-60,Shimadzu), Scanning Electron Microscopy (SEM, JEOL JSM-6500 F), SEM (JEOl 6360LVSEM), Energy Dispersive Spectroscopy (EDS, INCA 6360LVSEM), Two-probe resistivity setup (Scientific Equipment and Services, Roorkee), and Impedance Spectroscopy (Wayne Kerr Precision Component Analyzer 6440 B).

3 Results & discussion

Droplets in an emulsion (*w/o* and *o/w* i.e. oil in water) are known to be relatively large for low surfactant concentrations, much below their *CMC* (critical micelle concentration), and become significantly small when the surfactant concentration just reaches or exceeds *CMC* [23, 24]. In sol–gel emulsion system (*w/o*) this phenomenon offers a scope to tailor the shape and size of the gel particles [14]. Size of the water pools varies with the aggregation number of the surfactant molecules in the micelle and the relative quantity of the water phase [23, 24]. The micelles in *w/o* emulsions are known to have much smaller aggregation numbers than those in *o/w* types [24]. For surfactant concentrations exceeding *CMC*, the shape changes have been reported to vary from spherical to rod-like to uneven stumpy forms [23–26]. Span 80 or sorbitan monooleate ($C_{24}H_{44}O_6$) and span 20 or sorbitan monolaurate ($C_{18}H_{34}O_6$) were used as the non-ionic surfactants in the emulsion during synthesis to enhance the emulsion formation. The activity of the non-ionic surfactants is unaffected with parameters such as the pH, counter ions or the solvents [25]. The Hydrophilic-Lipophilic-Balance (*HLB*) that gives the total hydrophilic content in the surfactant molecule of these fatty acids are 4.3 and 8.6 for span 80 and span 20 respectively [27] . This indicates that span 80 is more soluble in organic solvents than span 20 [28, 29]. Role of these surfactants is to stabilize the emulsion by decreasing the interfacial tension between

the organic solvent and the sol that forms the emulsion, which in the present study is of *w/o* type. The inverse micelles act as templates to the sol droplets which are trapped within resulting into gel droplets after addition of triethylamine [26, 30]. The advantage of using inverse micelles over normal micelle is that the size of its aqueous micelle core is comparatively smaller with smaller aggregation number and it enhances the reaction rates [26, 31].

3.1 TGA, DSC analysis

The TGA curves for powders synthesized using Span 80 showed weight loss in three phases irrespective of the concentration of the surfactant used. The first phase was noted, between 35°C and 200°C, the second phase from 200°C to 450°C and the third phase from 500°C to 900°C. Figure 1(a) shows the TGA curve of the powder synthesized using 5% span 80. Weight loss in the first phase is caused by the evolution of water and other volatiles, in the second phase due to the combined effect of removal of organic components, hydroxyl group along with decomposition of acetate and the final weight loss is attributed to the decomposition of residual organics, intermediate phase formation like $BaCO_3$ and their reaction to form $BaTiO_3$ releasing CO_2 [32–36]. As seen from Fig. 1(a), first phase had a 60% weight loss followed by a 22% weight loss in the second phase and 3% weight loss in the third phase. Similar trend was observed for powders using span 20 as the surfactant, however, the weight loss in the corresponding temperature regions as before was 40%, 21% and 4% respectively.

Figure 1(b) shows the DSC curve of the powder synthesized using span 80, calcined at 750°C. No endothermic peak was observed at the transition temperature. DSC is known to be very sensitive to the phase change, and shows an endothermic peak at the tetragonal to cubic transition temperature of $BaTiO_3$ [17, 37]. As reported by Takeuchi et al. [17] the particle size increased with increasing sintering temperature, which in turn increased the tetragonality in the crystals. For powders showing tetragonality below 60% no such endothermic peak was observed and only at 64% a weak diffused peak was achieved. However, above 80% tetragonality a very distinct endothermic peak was obtained, with a transition enthalpy (ΔH) value of 200 J/mol for 95% tetragonality [17]. Xu et al. also reported the DSC peak for particles with a minimum of 80% tetragonality having ΔH value of 0.7–0.75 J/g [38]. A shift of T_c towards a higher value with increasing tetragonality in the samples was also noted [37]. The relation between ΔH and polarization (P) of the material is; $\Delta H = 2\pi P^2 T_c / C$, with C as the Curie-Weiss constant. This supports the fact that an increase in polarization achieved with higher tetragonality content will increase ΔH, which will be exhibited as an endothermic peak in the DSC profile [37, 39]. As the endothermic peak is absent in the DSC curves of the present work, it is clear that the percentage tetragonality in the synthesized powders is below 64%. Though high-permittivity and reliability is associated with the tetragonal structure, the sharp transition of permittivity at T_c restricts its application [40]. High-permittivity and stable dielectric constant for a large temperature range is required of a $BaTiO_3$ ceramic capacitor [41]. Hence a better control of the dielectric constant in the form of diffused transition is desired which can be achieved if the tetragonality is precisely controlled, and to do so, dopants are added so as to chemically modify the $BaTiO_3$ [17, 40, 41].

3.2 X-ray analysis

Figure 2(a) shows the XRD pattern of $BaTiO_3$ powders prepared by sol–gel emulsion technique with 5% span 80,

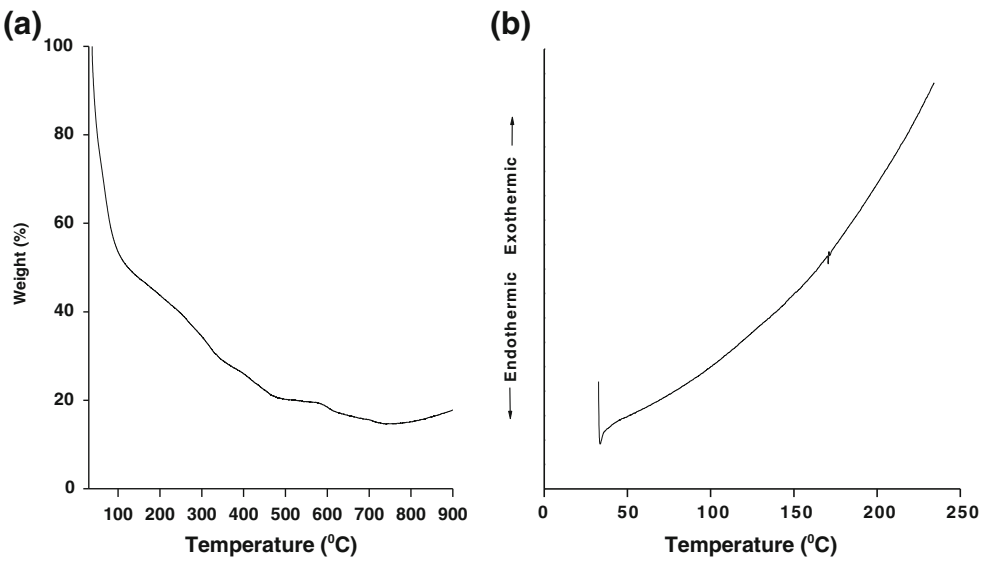

Fig. 1 $BaTiO_3$ powder synthesized for 5% span 80 (**a**) TGA curve, (**b**) DSC curve for the powder calcined at 750°C

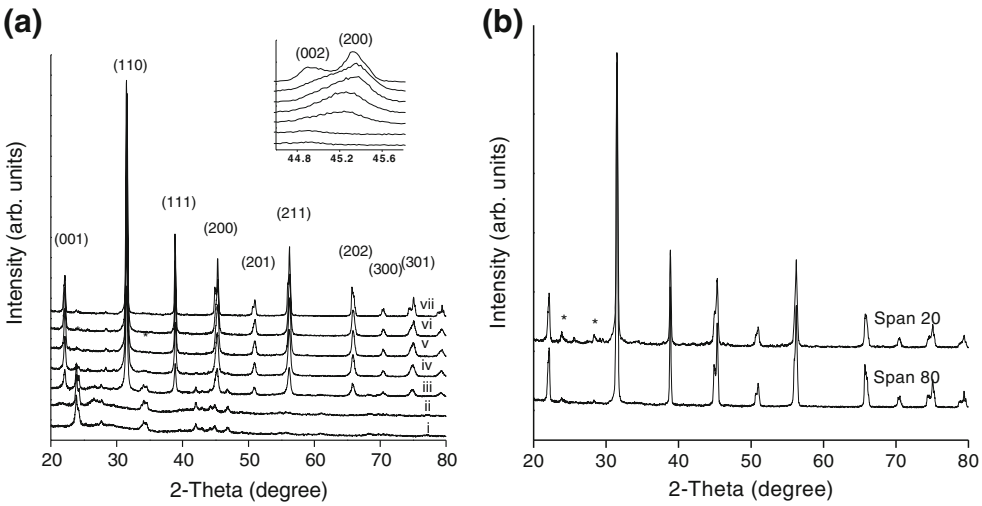

Fig. 2 X-ray diffraction pattern of $BaTiO_3$ synthesized (**a**) using 5% span 80 at temperatures (i) 400°C, (ii) 500°C, (iii) 600°C, (iv) 700°C, (v) 800°C, (vi) 900°C, and (vii) 1000°C. (**b**) using span 80 and 20 as the surfactant calcined at 1000°C (* - $BaCO_3$)

heat treated at 400°C, 500°C, 600°C, 700°C, 800°C, 900°C, and 1000°C. Single phased $BaTiO_3$, with traces of barium carbonate up to a calcination temperature of 700°C was observed. Crystalline peaks were observed above 400°C, and well developed peaks appeared from 600°C onwards. There was no distinct splitting of the (200) peak up to a calcination temperature of 900°C indicating the predominance of the cubic phase [38, 42–44]. However, a shoulder around (002) was noted in the powders calcined above 800°C. The (200), (002) peak distinction was clearly visible for the 1000°C calcined powder as seen in the inset of Fig. 2(a). Splitting of this peak confirmed the presence of the tetragonal phase in these powders. Micrometer size particles synthesized via. solid-state method, mechano-chemical method or hydrothermal method, under specific heat treatment cycles and calcination temperatures above 900°C showed the presence of tetragonal phase [17, 37–39]. Percentage tetragonality was found to reduce for particles below micrometer size, depending on the synthesis route, calcination temperature and cycle. With the decreasing particle size, the smaller domain sizes may have forced the unit cells to have pseudocubic symmetry resulting in the percentage of the tetragonal phase to reduce and that of the cubic phase to increase [17, 34]. Tetragonal $BaTiO_3$ powders are known to have higher density due to better sintering behaviour and larger permittivity values than the cubic powders that leads to their applications in MLCC [45]. However the paraelectric phase of $BaTiO_3$ shows better temperature stability of the dielectric constant at low temperatures at low AC field [40].

As seen from Fig. 2(b), $BaTiO_3$ powders synthesized using span 80 as the surfactant, calcined at 1000°C did not show any traces of $BaCO_3$. However, the same was present in the samples synthesized using span 20. This may be attributed to the different shapes of micelles formed in the two cases. The amount of tetragonality present in the powders was calculated using the method described by Takeuchi et al. [17], and was found to be 48% for span 80 and 23% for span20 surfactant used. It may be suggested that the presence of $BaCO_3$ interrupt the ordering of tetragonal domains leading to the material exhibiting a pseudo-cubic phase. Trace of $BaCO_3$ in span 20 powders is most probably the reason for its low tetragonality compared to span 80.

Average crystallite size of the particles were calculated using the Debye-Scherer formula,

$$d = 0.9\lambda/\beta\cos\theta$$

where, λ is the wavelength of the target used (λ=1.5405 Å, Cu K_α), $\beta=\sqrt{(B_m^2 - B_s^2)}$, B_m is the FWHM of the sample analyzed, B_s is the FWHM of the standard sample analyzed, θ is the Bragg angle of the 100% intensity peak, (Fig. 2(a)). The average crystallite size calculated for varying surfactant concentrations is shown in Table 1. For 750°C calcined

Table 1 Average crystallite size calculated for 1:3 sol:support solvent ratio and various surfactant concentrations

Emulsion Concentration		Calcination Temperature (750°C)		Calcination Temperature (1000°C)	
Sol: Support Solvent Ratio	Surfactant Volume	Span 80	Span 20	Span 80	Span 20
1:03	5%	27.93	24.02	45.00	43.05
	10%	29.85	30.92	44.01	46.82
	15%	30.37	31.64	45.70	47.99
	20%	33.03	35.51	44.01	52.01

powders the size varied from 27–33 nm for span 80 and 24–35 nm for span 20. Size variation for 1000°C calcined powders was 44–45 nm for span 80 and 43–52 nm for span 20.

3.3 SEM and EDS analysis

Figure 3 shows the SEM micrographs of the powders calcined at 750°C, for the two surfactants with varying

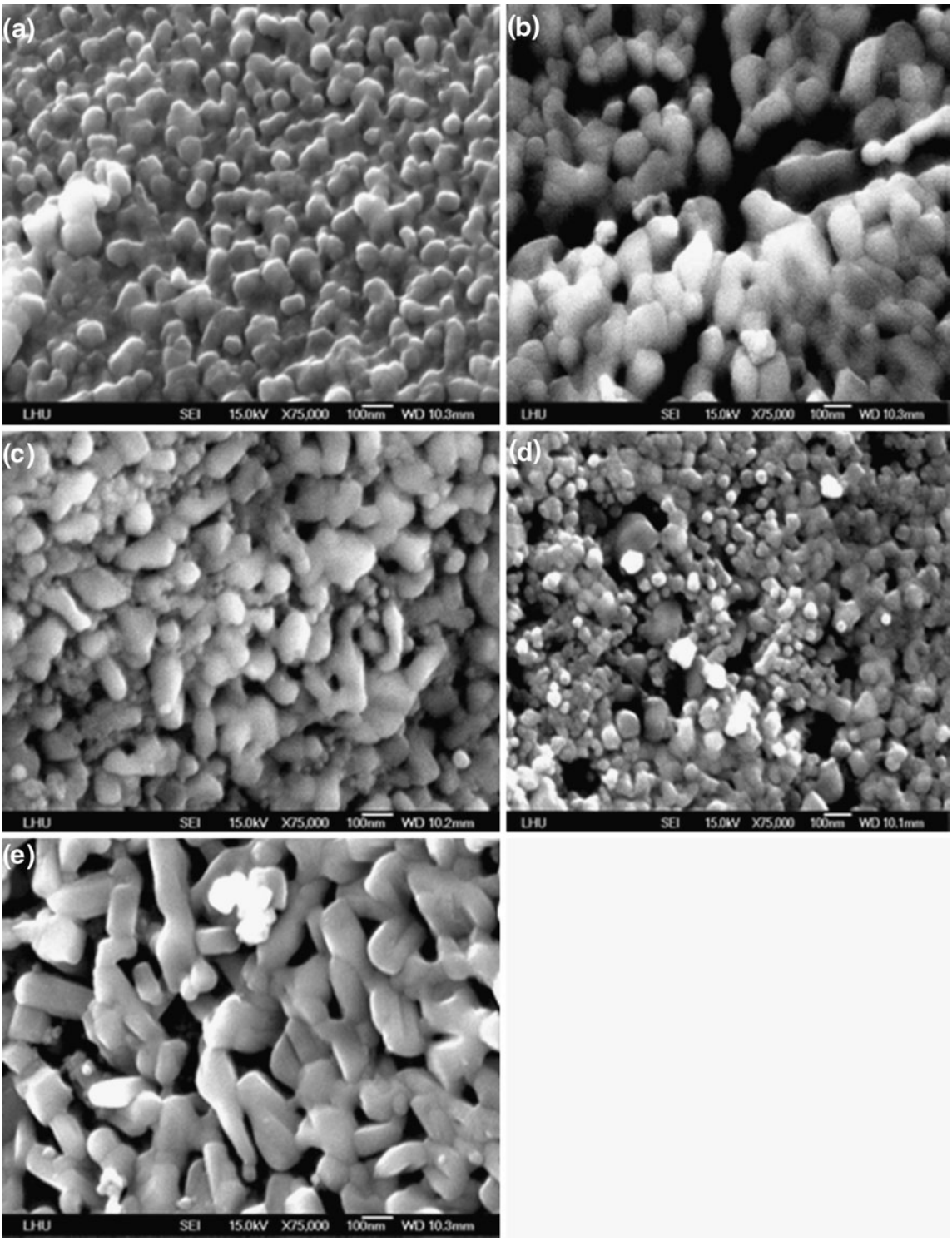

Fig. 3 SEM-$BaTiO_3$ morphology for powder calcined at 750°C using, (**a**) 5% span 80, (**b**) 10% span 80, (**c**) 15% span 80, (**d**) 20% span 80, and (**e**) 20% span 20

concentrations prepared. For Span 80, as the concentration was increased as 5 (Fig. 3(a)), 10 (Fig. 3(b)) and 15 (Fig. 3 (c)) vol%, the particle shapes changed from spherical to less spherical nature with some irregular structures. For 20 Fig. 3 (d)) vol% concentration, very small regular spherical particles were dispersed with more irregular shaped agglomerated particles. The SEM micrograph of powders prepared with span 20 (Fig. 3(e)) showed development of elongated structures instead of spheres. These particles were either rectangular or rod like in nature. As already known, the micelle shape depends on the concentration of the surfactant used and its *HLB* value gives information about its solubility [28]. For the non-ionic surfactants, the *HLB* value is also related to the *CMC* and the critical packing parameter (*CPP*) [30]. *CMC* increased and *CPP* decreased with increasing *HLB* value. *CPP* value of span 80 is greater than 1 [46]. Span 20 having a higher *HLB* value than span 80, will have a smaller *CPP* value. For a normal micelle the structure is reported to change from spherical to lamellar with increasing *CPP*, however, for the reverse micelle, a higher *CPP* promotes the formation of spherical inverse micelle [30]. Hence, with comparatively lower *CPP* than span 80, span 20 surfactant concentration used is most probably not enough to form spherical structure and form the rod-like micelles. Whereas, the span 80 concentration used is enough for the spherical inverse micelle formation [25, 28, 30, 46]. These micelles act as templates for the $BaTiO_3$ particles that take the same shape.

The size of the particles as a function of surfactant and its concentration were calculated from the SEM micrographs shown in Fig. 3. The average values reported here were calculated using 50 grains which included the smallest and the largest particles observed in each micrograph. For 5 vol. % span 80 most of the particles were found to be in 30 to 70 nm size range with a few in the range of 90–100 nm, the average of which was calculated to be 57 nm. Similarly, for 10 vol.% span 80 most of the particles were in the 60–80 nm range with a few about 120 nm range having an average of 92 nm. 15 vol.% span 80 particles were equally distributed from 40 nm to 140 nm having an average size of 94 nm. However the size range of particles decreased when the span 80 concentration increased to 20 vol.%, and was found to be distributed from 15 nm to 80 nm averaging out as 42 nm. With 20 vol.% span 20, the particle size ranged from 18 to 125 nm averaging to 66 nm. No clear trend was hence observed between the surfactant concentration and the size of the particles. Figure 4(a) and (b) show the SEM micrographs of the pellets of the $BaTiO_3$ powders synthesized

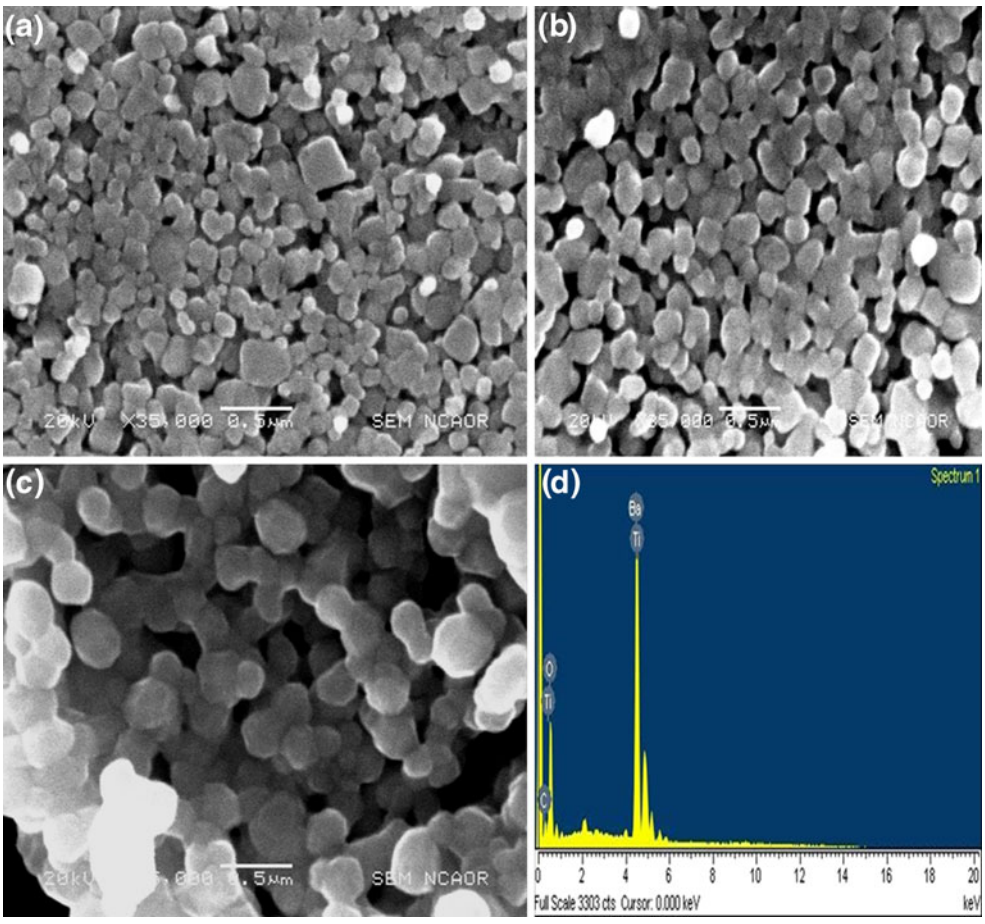

Fig. 4 Particle morphology of the pellets (5% span 80 powder) calcined at (**a**) 750°C for 1 h soaking, (**b**) 750°C for 12 h soaking and (**c**) 1200°C for 2 h soaking (**d**) EDS spectrum (750°C for 1 h soaking)

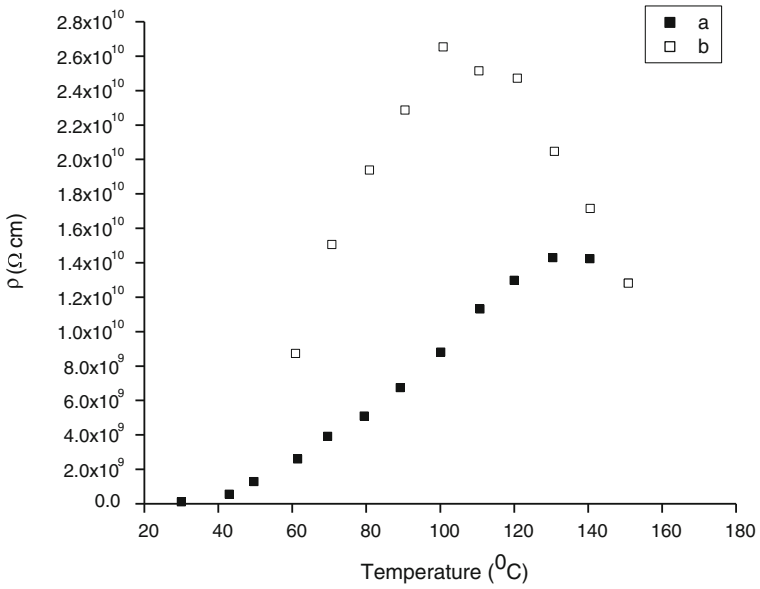

Fig. 5 PTCR effect in doped $BaTiO_3$ for 5% span 80 heat treated at 750°C during the (**a**) heating and (**b**) cooling cycle

using 5% span 80 calcined at 750°C, sintered at 750°C with a soaking time of 1 h and 12 h respectively. Figure 4(c) shows the micrograph of the pellet prepared from the same powder but sintered at 1200°C for 2 h. The micrographs showed grain growth and formation of neck between adjacent grains, as expected with increase in sintering temperature and soaking time [47]. The EDS spectrum in Fig. 4(d), confirmed the presence of Ba, Ti and O in the synthesized material.

3.4 Resistivity analysis

Figure 5 shows PTCR effect for $BaTiO_3$ pellet sintered in ambient conditions. Resistivity measurement was carried out during the heating and cooling cycle on the pellet sintered at 750°C (made from powders initially calcined at 750°C). The resistivity values changed from~10^8 Ωcm to 10^{10} Ωcm. Figure 5 shows the T_c (Curie point) of the pellets to be approximately 75°C, as calculated from the variation of slope with temperature of the resistivity vs. temperature curve. Curie point has been reported to decrease from the value of 120°C observed for ideal $BaTiO_3$ crystals, with decrease in particle sizes [34]. $SrTiO_3$, $CaZrO_3$ etc., known as T_c shifters, are added to $BaTiO_3$ to shift the T_c to higher or lower values as intended [1]. Lower T_c is desired to obtain higher permittivity values at lower temperatures [1]. The values recorded during cooling cycle had resistivity values higher than that recorded for heating cycle (Fig. 5). A similar behavior of high resistivity during the cooling cycle was observed by Kim et al. [48], when the samples were analyzed in the oxygen atmosphere. They attributed this to the small increase in potential barrier due to the decrease in number of conduction electrons because of adsorbed oxygen at grain boundaries.

Pure $BaTiO_3$ is usually an insulator with no PTCR effect [49]. Semiconducting doped $BaTiO_3$ deviates from its insulating behavior either when (1) it is doped with donors, (2) when gases are adsorbed on the surface of the grains or (3) when cation vacancies are created. Resistivity of semiconducting $BaTiO_3$ increases at T_c due to the acceptor levels/

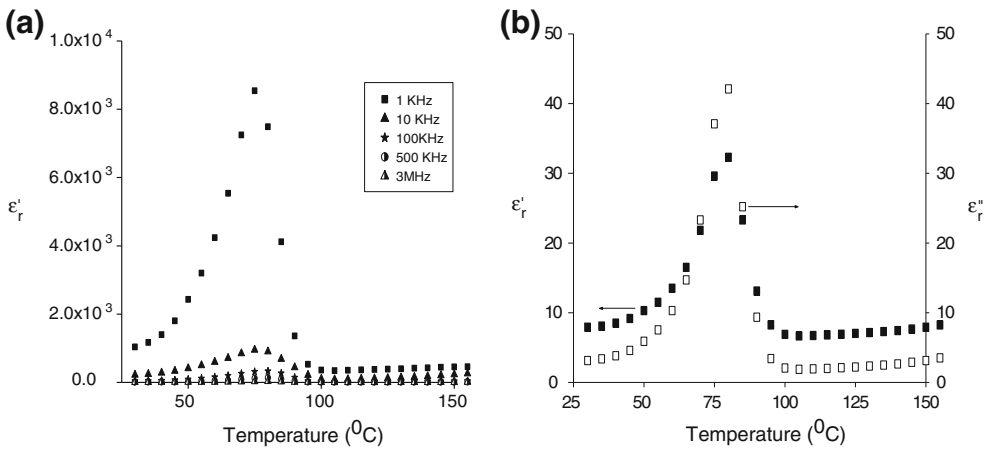

Fig. 6 $BaTiO_3$ dielectric response for 5% span80 sample sintered at 750°C (12 h soaking), measured at (**a**) fixed frequencies, and (**b**) 3 MHz frequency

electron traps created by either of the above mentioned methods resulting in the potential barrier increase at the grain boundaries [14–16]. Each PTCR-$BaTiO_3$ grain possesses heterogeneous electrical properties due to the presence of a core of pure ferroelectric $BaTiO_3$ surrounded by a paraelectric shell containing the dopant [9, 40]. However, in the present paper PTCR behavior was noted in undoped $BaTiO_3$ samples. The most possible reason is due to the size range of the particle which makes the material predominantly cubic at room temperature. PTCR behavior is normally associated with the presence of paraelectric cubic phases [13, 40]. Cation vacancies if present during sintering may also possibly contribute towards the observed PTCR characteristics [49].

3.5 Impedance spectroscope analysis (IS)

Dielectric property of $BaTiO_3$ was measured by impedance spectroscopy using the pellet, made from powders calcined at 750°C, sintered at 750°C for 12 h of soaking time. Figure 6(a) shows a permittivity vs. temperature behavior that is typical of a ferroelectric $BaTiO_3$ for different frequencies. Figure 6(b) shows the real and imaginary dielectric constant for the same pellet at 3 MHz frequency. For a frequency of 1 kHz the permittivity maximum was observed at 75°C which is same as the T_c noted from the resistivity curves. With an increase in the frequency to 3 MHz the T_c shifted to 80°C. Similar shift in value of T_c with changes in frequency, has been noted by several researchers for doped $BaTiO_3$ ceramics which they associated with the increase in the relaxor behaviour of the material [50–54]. Maximum value of permittivity obtained for 1 kHz frequency at T_c is 9000, which decreases with increasing frequency to as low as 33 for the 3 MHz frequency. Values of dielectric constant from 600 to 12000 has been reported for $BaTiO_3$ prepared by various synthesis methods and having various particle size ranges [17, 38, 50]. As seen from the Fig. 6(b), with an increase in the dielectric constant, losses in the material also increased at 3 MHz frequency. Dielectric constant (ε_r) of a normal ferroelectric decreases with increasing frequency as it becomes difficult for the domains to change their orientation at the same rate as that of the electric field [55, 56].

4 Conclusion

The sol–gel emulsion technique used in this work shows that the as synthesized powder needs to undergo a heat treatment to crystallize into $BaTiO_3$. Below calcination temperature of 800°C $BaCO_3$ exists as an impurity in the calcined powders as seen for the span 80 samples. However, the impurities were sustained in the powders synthesized using span 20 even at 1000°C calcination temperature. Microstructure of the synthesized powders formed into a spherical structure for a low surfactant concentration of 5 vol.% span 80, which when increased, distorted the shape of the synthesized powders. PTCR effect is obtained for the powders calcined in ambient conditions, with values as high as 1×10^{10} Ωcm. The absence of the endothermic peak (DSC) characteristic of the phase transition from tetragonal to the cubic is due to the small particle size due to which tetragonal structure formation was incomplete and a high amount of cubic structure sustained in the samples [17, 37, 49]. A critical size of the crystal lattice exists both, above and below which the crystal lose their polarizability due to which a decrease in permittivity is seen. It is clear from various studies that the permittivity of the material depends on the particle size [17, 50, 55, 57]. Well investigated is the fact that PTCR is a grain boundary phenomenon [13, 48, 58, 59]. Potential barriers are formed at the grain boundary by creating acceptor states at the surface of the ferroelectric grain. The acceptor states can either be the adsorbed oxygen or the intrinsic cation vacancies or both formed during the heat treatments. Hence, the decrease in the T_c to near room temperature in our samples is attributed to the particle size which does not favor complete tetragonal structure formation due to which a non-ferroelectric phase exists that results in the increase in resistivity at T_c i.e. PTCR behavior.

Acknowledgment The present work was funded by the Defense Research and Development Organization (DRDO). We would like to thank Dr. N. N. Ghosh (BITS, Pilani – K. K. Birla Goa Campus) for TGA and DSC analysis, Dr. Rosilda Selvin (Lunghwa University Taiwan) for the SEM analysis, Dr. Rahul Mohan (NCAOR, Goa) for the SEM and EDS analysis and Dr. Tangsali (Goa University) for the Impedance Spectroscopy analysis.

References

1. H.H. Gene, J. Am, Ceram. Soc. **82**(4), 797–818 (1999)
2. A.J. Moulson, J.M. Herbert, *Electroceramic: Materials, Properties and Applications*, 2nd edn. (Wiley, Chichester, 2003), p. 91
3. C.D. Chandler, C. Roger, M.J. Hampden-Smith, Chem. Rev. **93**, 1205–1241 (1993)
4. S.B. Narang, D. Kaur, Ferroelectr. Lett. Sect. **36**, 20–27 (2009)
5. E. Aksel, J.L. Jones, Sensors **1**, 1935–1954 (2010)
6. R.M. Glaister, H.F. Kay, Proc. Phys. Soc. IOP Science **76**, 763 (1960)
7. A. Jamal, M. Naeem, Y. Iqbal, J. Pak, Mater. Soc. **2**(2), 91–95 (2008)
8. W.H. Lee, C.Y. Su, J. Am, Ceram. Soc. **90**(10), 3345–3348 (2007)
9. P. Fiorenza, R.L. Nigro, P. Delugas, V. Raineri, A.G. Mould, D.C. Sinclair, Appl. Phys. Lett. **95**, 142904 (2009)
10. F. Gebhard, *The Mott Metal-Insulator Transition: Models and Methods*, vol. 137 (Springer, Verlag, Berlin, 2000), pp. 1–48. STMP
11. Y.X. Li, X. Yao, L.Y. Zhang, J. Electroceram. (2007). doi:10.1007/s10832-007-9242x
12. S. Chatterjee, B.D. Stojanović, H.S. Maiti, Mater. Chem. Phys. **78**, 702–710 (2003)

13. S. Hishita, J.F. Baumard, P. Abelard, Colloq. Phys. **51**, 979–984 (1990)
14. M. Chatterjee, M.K. Naskar, D. Ganguli, J. Sol-Gel Sci. Technol. **16**, 143–149 (1999)
15. S. Srimala, F.M.N. Ahmad, A.A. Zainal, O. Radzali, W. Anthony, J. Mater. Process. Tech. **195**, 171–177 (2008)
16. V.P. Pavlović, B.D. Stojanović, V.B. Pavlović, L. Živković, M.M. Ristić, Sci. Sinter. **34**, 73–77 (2002)
17. T. Takeuchi, M. Tabuchi, K. Ado, K. Honjo, O. Nakamura, Y. Suyama, N. Ohtori, M. Nagasawa, J. Mater. Sci. **32**, 4053–4060 (1997)
18. N.J. Joshi, G.S. Grewal, V. Shrinet, A. Pratap, N.J. Buch, Integr. Ferroelectr. **115**, 142–148 (2010)
19. F. Valdivieso, M. Pijolat, M. Soustelle, Chem. Eng. Sci. **51**(11), 2535–2540 (1996)
20. U.Y. Hwang, H.S. Park, K.K. Koo, J. Am, Ceram. Soc. **87**(12), 2168–2174 (2004)
21. C. Pithan, Y. Shiratori, R. Waser, J. Dornseiffer, F.-H. Haegel, J. Am, Ceram. Soc. **89**(9), 2908–2916 (2006)
22. V. Devarajan, V. Ravichandran, Int. J. Comprehensive Pharmacy **4** (1) (2011)
23. M. Bourel, R.S. Schecter, *Microemulsions and Related Systems* (Marcel Dekker, New York, 1998)
24. E. Dickinson, in *Controlled Particle, Droplet and Bubble Formation*, ed. by D.J. Wedlock (Butterworth-Heinemann, Oxford, 1994), p. 204
25. J. Zhang, Z.-L. Wang, J. Liu, S. Chen, G.-Y. Liu, in *Nanostructure Science and Technology: In Self-Assembled Nanostructures*, ed. by J.D. Lockwood (Kluwer Academic/Plenum Publishers, New York, 2003). Chapter 2
26. L.K. Shrestha, T. Sato, R.G. Shrestha, J. Hill, K. Ariga, K. Aramaki, Phys. Chem. Chem. Phys. **13**, 4911–4918 (2011)
27. B.K. Paul, R.K. Mitra, J. Colloid Interface Sci. **288**, 261–279 (2005)
28. L.L. Schramm (ed.), *Surfactants: Fundamental and Applications in the Petroleum Industry* (Cambridge University Press, United Kingdom, 2000)
29. S. Smitha, P. Shajesh, P. Mukundan, K.G.K. Warrier, J. Sol-Gel Sci, Technol. **48**, 356–361 (2008)
30. Inderjit (ed.), *Weed Biology and Management* (Kluwer Academic Publishers, Netherlands, 2004)
31. U. Natarajan, K. Handique, A. Mehra, J.R. Bellare, K.C. Khilar, Langmuir **12**, 2670–2678 (1996)
32. H.P. Beck, W. Eiser, R. Haberkorn, J. Eur, Ceram. Soc. **21**(6), 687–693 (2001)
33. P. Durán, F. Capel, J. Tartaj, D. Gutierrez, C. Moure, Solid State Ionics **141–142**, 529–539 (2001)
34. Y. Zhang, S. Luo, Y. Fu, K. Zhang, J. Mater. Sci. **41**, 3179–3182 (2006)
35. A. Kareiva, S. Tautkus, R. Rapalaviciute, J.-E. Jørgensen, B. Lundtoft, J. Mater. Sci. **34**, 4853–4857 (1999)
36. B.L. Newalkar, S. Komarneni, H. Katsuki, Mater. Res. Bull. **36**, 2347–2355 (2001)
37. R. Asiaie, W. Zhu, A.A. Sheikh, P.K. Dutta, Chem. Mater. **8**, 226–234 (1996)
38. H. Xu, L. Gao, J. Am, Ceram. Soc. **86**(1), 203–205 (2003)
39. B.M. Gorelov, E.V. Kotenok, S.N. Makhno, V.V. Sydorchuk, S.V. Khalameida, V.A. Zazhigalov, Solid-State Electron. **56**(1), 83–91 (2011)
40. K. Yasukawa, M. Nishimura, Y. Nishihata, J. Mizuki, J. Am, Ceram. Soc. **90**(4), 1107–1111 (2007)
41. S.-H. Yoon, J.-H. Lee, D.-Y. Kim, N.M. Hwang, J. Am, Ceram. Soc. **86**(1), 88–92 (2003)
42. J.-M. Hwu, W.-C. Yu, Y.-W. Chen, Y.-Y. Chou, Mater. Res. Bull. **40**, 1662–1679 (2005)
43. N.G. Devaraju, B.I. Lee, X. Wang, M. Vivani, P. Nanni, J. Mater. Sci. **41**, 3335–3340 (2006)
44. Y. Xie, S. Yin, T. Hashimoto, Y. Tokano, A. Sasaki, S. Tsugio, J. Mater. Sci. (2009). doi:10.1007/s10853-009-3991-9
45. W. Zhu, S.A. Akbar, R. Asiaie, P.K. Dutta, J. Appl. Phys. **36**, 214–21 (1997)
46. T. Schmidts, D. Dobler, C. Nissing, F. Runkel, J. Colloid Interface Sci. **338**, 184–192 (2009)
47. W.D. Callister Jr., *Materials Science and Engineering: An Introduction*, 6th edn. (Wiley, Singapore, 2006), p. 444
48. J.-G. Kim, J. Mater. Sci. Lett. **21**, 1645–1647 (2002)
49. B. Huybrechts, K. Ishizaki, M. Takata, J. Mater, Sci. **30**, 2463–2474 (1995)
50. N. Masó, H. Beltrán, E. Cordoncillo, D.C. Sinclair, A.R. West, J. Am, Ceram. Soc. **91**(1), 144–150 (2008)
51. U.A. Joshi, S. Yoon, S. Baik, J.S. Lee, J. Phys, Chem. B **110**, 12249–12256 (2006)
52. A.H. Elsayed, A.M. Haff, Egypt. J. Solids **28**(1) (2005)
53. M. Zhu, L. Liu, Y. Hou, H. Wang, H. Yan, J. Am, Ceram. Soc. **90** (1), 120–124 (2007)
54. X. Chou, J. Zhai, X. Yao, J. Am, Ceram. Soc. **90**(9), 2799–2801 (2007)
55. M. Aparna, T. Bhimasankaram, S.V. Suryanarayana, G. Prasad, G. S. Kumar, Bull. Mater. Sci. **24**(5), 497–504 (2001)
56. C. Elissalde, J. Ravez, J. Mater, Chem. **11**, 1957–1967 (2001)
57. B. Garbarz-Glos, R. Bujakiewicz-Korońska, D. Majda, M. Antonova, A. Kalvane, C. Kuś, Intergrated Ferroelectrics **108**, 106–115 (2009)
58. H.T. Kim, Y.H. Han, Ceram. Int. **30**(7), 1719–23 (2004)
59. D. Makovec, M. Drofenik, J. Baker, J. Am, Ceram. Soc. **86**(3), 495–500 (2003)